A STEPWISE, ITERATIVE PROCEDURE TO CONSTRAIN STRESS DROP, REGIONAL ATTENUATION MODELS, AND SITE EFFECTS

Mark D. Fisk[1] and W. Scott Phillips[2]

Alliant Techsystems[1] and Los Alamos National Laboratory[2]

Sponsored by the Air Force Research Laboratory[1] and the National Nuclear Security Administration[2]

Contract Nos. FA8718-09-C-0005[1] and LA09-BAA09-01-NDD03[2]
Proposal No. BAA09-01

ABSTRACT

Accurate corrections for distance, source size, and site effects are needed for reliable use of regional seismic phases for discrimination and magnitude estimation. Procedures that simultaneously invert for attenuation, geometrical spreading, site, and source parameters have been shown to include many trade-offs and instabilities that have led to significantly inaccurate corrections for distance and source terms. Under previous work, we developed and applied an approach to constrain source parameters, including stress drop, for events throughout Eurasia, using Brune (1970) model fits to relative spectra of regional phases for event pairs with similar locations and mechanisms (assessed by waveform correlations), but different moments. We further fit the combined distance and site terms to the source-corrected spectra, showing that robust estimates of these combined effects are possible by first constraining source terms. Further work is needed to separately constrain the path and site effects. We have just started a three-year project to implement, apply, and evaluate a stepwise, iterative procedure to constrain all of the remaining trade-offs among these terms. Using spectra of regional seismic phases that are already corrected for source terms, we will estimate and apply corrections for frequency-independent geometrical spreading and site factors, based on distance, and then constrain separate estimates of frequency-dependent site parameters and Q. This is expected to provide accurate estimates of all source, distance, and site effects for regional phases in Eurasia for paths/stations with suitable data. We also plan to use coda measurements and methods to (1) augment our source terms computed from spectra of direct phases, (2) independently estimate site terms, and (3) compare and validate the results using direct phases or coda. We will use analysis of variance (ANOVA) and variogram methods to partition the uncertainties and their correlation lengths for use in Bayesian kriging to interpolate grids of stress drop, geometrical spreading, and Q estimates, and to merge our results with previous developments at Los Alamos National Laboratory (LANL). We will evaluate the corrections and uncertainties using two large data sets and cross-validation methods. We will document and deliver the techniques, estimates of physical parameters, and kriged grids of corrections and uncertainties, for incorporation in the Air Force Technical Applications Center Knowledge Base.

OBJECTIVES

We have just started a project to develop, apply, and evaluate methods to improve the accuracy of attenuation models, geometrical spreading, site terms, and their uncertainties for regional phases in Eurasia, by constraining trade-offs among the parameters at various stages of the analysis. The approach is to break up traditional grid-search inversions, which are known to have many trade-offs and instabilities, into manageable pieces, canceling out certain physical effects (e.g., distance and site) to allow reliable estimation of others (e.g., source), and then correcting for the latter to then estimate reliable parameters for the former. We plan to use complementary datasets based on direct phases and coda measurements to augment and compare source terms and independently estimate site terms. We also plan to use multiple methods to estimate the correction parameters and to validate the results at key stages. We will partition the uncertainties and their correlation lengths for use in Bayesian kriging to interpolate grids of stress drop, geometrical spreading, and Q estimates, and to merge our results with previous developments at LANL. We will evaluate the corrections and uncertainties using two large datasets and cross-validation methods.

RESEARCH ACCOMPLISHED

Procedures that simultaneously invert (i.e., grid search) for Q, geometrical spreading, site, and source parameters have been shown (e.g., Taylor and Hartse, 1998; Fisk and Taylor, 2006; Fisk et al., 2008) to have many trade-offs and instabilities that have led to significantly inaccurate corrections. This motivated our development of an approach to better constrain the parameters. Under previous work, we developed and applied a method to constrain source parameters, including stress drop, for events throughout Eurasia, using Brune (1970) model fits to relative spectra of regional phases for event pairs with similar locations and mechanisms (assessed by waveform correlations), but different moments. We then corrected the spectra for the source terms and fit the combined distance and site effects, showing that robust estimates of these combined terms are possible by first constraining source terms. Further work is planned to separately constrain path and site effects. Here we summarize relevant past work and plans for this project.

Constrained Inversion Approach

Following Sereno et al. (1988), Taylor and Hartse (1998), and Taylor et al. (2002), the amplitude spectrum for a given phase and station, for event i, may be modeled by

$$A_i(f) = S_i(f;f_c(\sigma_b^{(0)}, \psi))G(r_i;r_0, \eta)\exp\left(-\frac{\pi f^{1-\gamma}}{Q_0 \nu} r_i\right)P(f;a, b) \quad \text{(EQ 1)}$$

where $S_i(f,f_c)$ is the source spectrum with corner frequency f_c, r_i is epicentral distance, $P(f)$ is the site term, ν is group velocity, $Q_0 f^{\gamma}$ treats attenuation, and $G(r, r_0)$ is frequency-independent geometrical spreading, inversely proportional to distance to a power η, beyond a reference distance r_0. Taylor et al. (2002) and many others have used the logarithm of Equation (1) in grid searches to simultaneously estimate all of the parameters. However, significant trade-offs among the parameter estimates are well known and difficult to constrain by such techniques and available data. The problem arises because the earth and the distribution of events and stations are not uniform.

Figure 1 illustrates the problem for two earthquakes at the Lop Nor test site (LNTS). It shows ratios of Pn, Sn, and Lg spectra for the larger event (M_W 5.7) relative to the smaller (M_W 4.4), computed at 18 stations and averaged. The events have similar hypocenters and mechanisms; thus path, site, and radiation pattern effects cancel in the relative spectra. Also shown are Brune (1970) model predictions using stress drop estimates from (1) an unconstrained grid search (Taylor et al., 2002) and (2) our fits of the relative spectra. The unconstrained result clearly does not match the observed relative spectra. Also, using our fits of the source terms, Figure 2 compares the source-corrected Lg spectra at MAKZ for the same earthquakes to Q model predictions from (1) unconstrained MDAC parameters and (2) our fit. The unconstrained result diverges by over an order of magnitude at higher frequencies. A trade-off of Q and stress

drop for the unconstrained grid search leads to very inaccurate corrections for both.

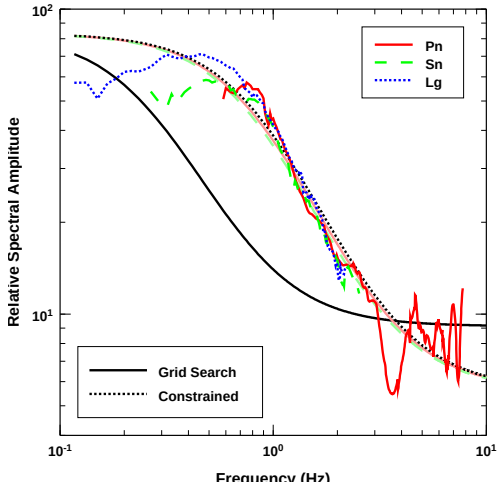

Figure 1. Station-averaged relative spectra of Pn, Sn, and Lg for a pair of earthquakes (M_W 5.7 and 4.4) at LNTS. Also shown are Brune model results using stress drop estimates from an unconstrained grid search (black) and our fits of the relative spectra.

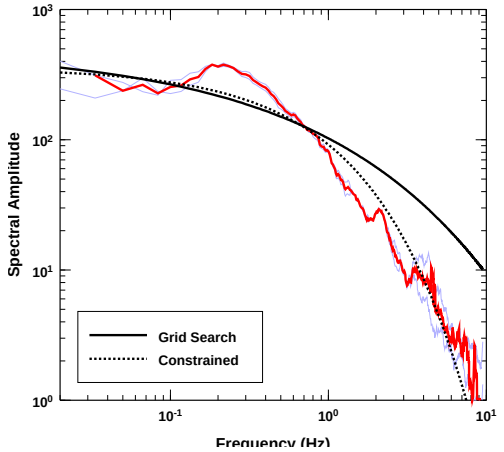

Figure 2. Source-corrected Lg spectra for the LNTS earthquakes at MAKZ, the result using Q from a grid search (solid), and our Q model fit (dotted).

This case not only illustrates the problem, but also a solution. Instead of performing a grid search for all parameters simultaneously, we use relative spectra for event pairs with similar locations and focal mechanisms (assessed by waveform cross-correlations), but different moments, to factor out path and site effects and obtain reliable estimates of the source terms. Once accurate source terms are estimated, we can then obtain reliable estimates of the distance and site terms. That is, for a pair of nearby earthquakes with similar radiation patterns, the relative spectra for a given phase type is modeled by

$$\frac{A_1(f)}{A_2(f)} = \frac{S_1(f)}{S_2(f)} = \frac{M_0^{(1)}[1+(f/f_c^{(2)})^2]}{M_0^{(2)}[1+(f/f_c^{(1)})^2]} \quad . \qquad \text{(EQ 2)}$$

The corner frequency may be parameterized in terms of moment M_0, stress drop $\sigma_b^{(0)}$, and a scaling parameter ψ. Using pairs of similar earthquakes, we fit $\sigma_b^{(0)}$ and ψ to relative spectra. Figure 3 shows network-averaged relative spectra and model fits for an earthquake pair in Kyrgyzstan during 1997. The relative spectra are similar for the various phases, although over different frequency ranges because of phase-dependent SNR effects. Hence, the corner frequencies are very similar, a common and important phenomenon for the earthquakes analyzed.

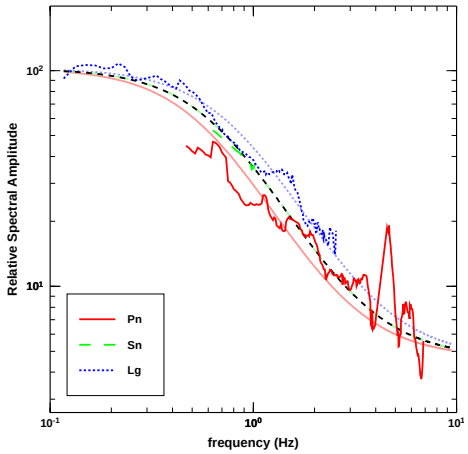

Figure 3. Example of relative spectra for a pair of M_W 6.0 and 4.7 earthquakes. Model fits are shown for each phase and using all phases (black dashed).

For this approach to be viable, many pairs are needed. Using waveform cross-correlations for 4,236 events in Eurasia prior to 2000 (Schaff and Richards, 2004) we found a subset of pairs in the LANL database, acquired data from IRIS, added/refined phase picks, computed and averaged relative spectra over stations, and fit the model for each phase and for all phases simultaneously. Figure 4 shows that Pn and Lg corner frequencies are similar for most of the earthquakes analyzed in Eurasia, comparable to findings by Walter and Taylor (2002) for western U.S. earthquakes. This allows more robust fitting of Brune source parameters, using a broader range of frequencies, by combining relative spectra of regional

P and S phases for earthquakes (e.g., black dashed curve in Figure 3). Figure 5 shows initial kriged grids of stress drop based on Lg and Pn data. The grids are very similar, indicating similar stress-drop estimates from Lg and Pn.

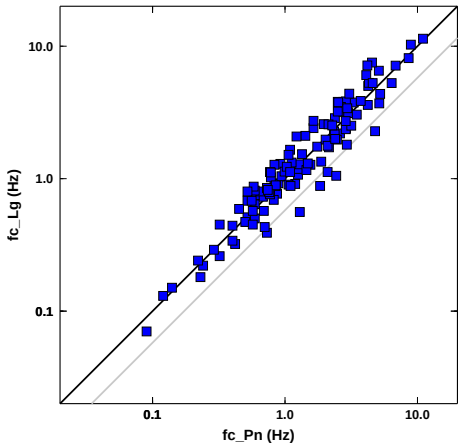

Figure 4. Estimated Lg versus Pn corner frequencies, indicating similar values for most of the earthquakes. Black and gray lines represent ratios of 1.0 and 1.73.

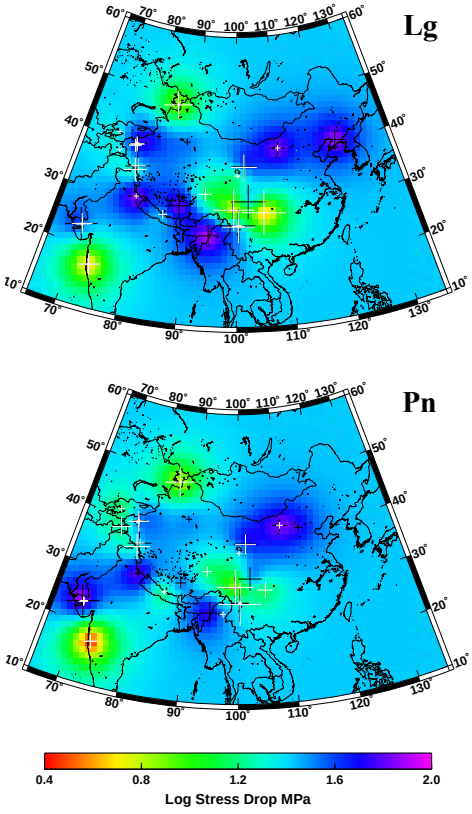

Figure 5. Initial kriged stress-drop grids estimated from Lg (top) and Pn (bottom) relative spectra.

We extended our analysis of relative spectra to event pairs in Eurasia from 2000 to 2006 (Figure 6). Using the Preliminary Determination of Epicenters (PDE) catalog, we formed a list of candidate pairs, based on proximity and relative mb or M_W values in the PDE, and acquired regional data for the events from IRIS. We computed waveform cross-correlations to find similar event pairs (*á la* Schaff and Richards, 2004). We computed and fit network-median relative spectra for almost 3600 pairs. We semi-automated these processing steps, although it is necessary to review and refine the results. In the fitting analysis, we fix M_0 of the larger event, assuming it is better recorded and, hence, has a more reliable moment estimate, and estimate M_0 of the smaller event.

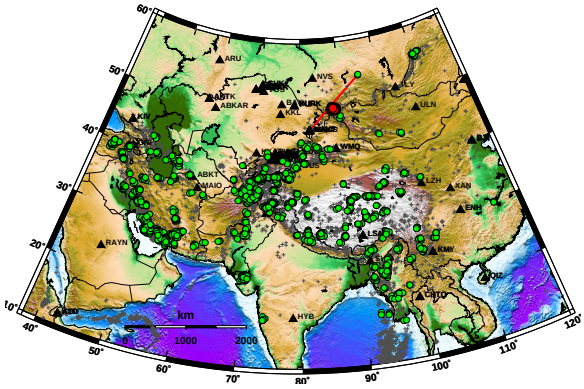

Figure 6. Events and stations used to process relative spectra and fit corner frequencies and estimate stress drop. The cluster highlighted in red and the path along two clusters to MAKZ are discussed below.

Figure 7 shows an example for a pair of the highlighted cluster in Figure 6. Figure 8 shows corner frequency estimates and their scaling relation for the entire cluster. Using the estimated source terms to correct the spectra, we fit the combined distance and site dependence. For example, Figure 9 shows source-corrected Lg spectra at BRVK for the cluster, illustrating several important aspects of our analysis. (Results were computed for 23 stations.) First, the light blue curves show the corrected Lg spectra for each event. They have similar shapes and offsets, indicating that the source corrections (moments and corner frequencies) are effective and consistent. Modest departures at low and high frequencies are due to noise effects. Second, the median (red curve) for the cluster is robust to outliers. For example, the lowest blue curve is due to a bad BRVK recording that slipped

through the automated QC criteria. The mean is much more sensitive to outliers. Third, the fit (black curve) of the median spectrum agrees very well over a wide range of frequencies. We generated comparable results for all of the stations and for other clusters/paths.

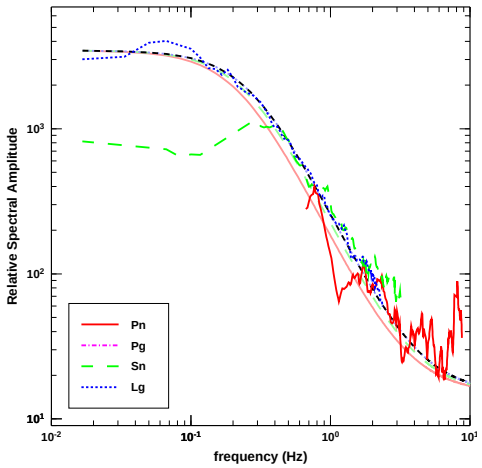

Figure 7. Network-median relative spectra of Pn, Sn, and Lg and model fits (smooth curves) for an event pair in the highlighted cluster in Figure 6.

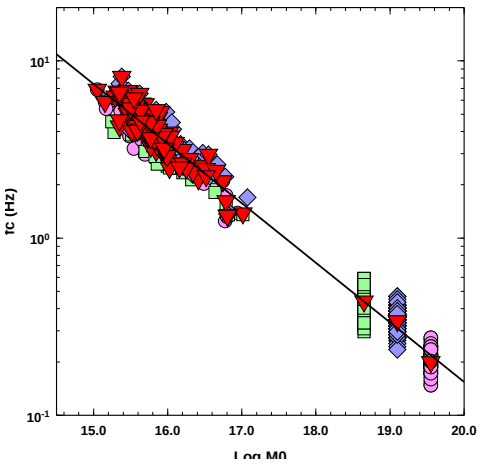

Figure 8. Corner frequencies versus log moment for the highlighted cluster in Figure 6, by jointly fitting the relative Pn, Sn, and Lg spectra. Estimates are shown for all pairwise combinations using 3 master events (circles, diamonds, squares), the median for each event (triangles), and the scaling relation (line).

The source parameters (Figures 7 and 8) and the dashed curve of Figure 9 provide excellent/complete calibration over a wide range of frequencies for all of the combined source distance, and site effects for this path/station. For an isolated cluster, the fits do not provide independent, reliable estimates of Q, spreading, and site parameters. New work focuses on constraining remaining trade-offs.

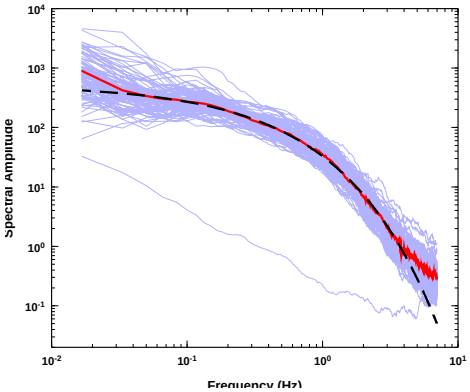

Figure 9. Lg spectra at BRVK, corrected for response and source terms, for all events in the cluster (blue), the median (red), and a model fit of the combined distance and site effects (black dashed).

Comparisons of Q Parameters

We compared our effective Q estimates to independent results. First, Dr. Jiakang Xie provided estimates of Q_0, computed as an integrated average of Q_0^{-1} along the same paths, using an Lg Q tomographic map generated by the two-station method (Xie et al., 2005, 2006). As a convenient way to compare the results, Figure 10 shows maps of Lg Q_0 estimates from our analysis and from Xie (2008, pers. comm.) for paths from the same cluster to 23 stations. The maps were generated by kriging and are only intended to aid visual comparisons. Compared to Xie's estimates, we obtain higher Q_0 estimates for paths to stations in northern Kazakhstan and, to a lesser extent, to stations in Kyrgyzstan, as well as a lower Q_0 estimate for the path to WMQ. The Q_0 estimates are comparable for the path to ULN. Further work is needed to evaluate and interpret these results, after separately estimating site effects. We do note that our estimates of Lg Q_0 for these stations seem to be more consistent with results by Taylor et al. (2003), specifically higher Q_0 for paths to northern Kazakhstan and lower Q_0 for paths to northwestern China.

For paths from LNTS to regional stations, we compared our Q_0 estimates for Pn, Sn, and Lg to those computed from averages of Q_0^{-1} along the paths using tomographic maps from Phillips (2005, pers. comm.). Our results

were generated using only one event pair at LNTS. Figure 11 shows source-corrected Lg spectra and model fits, giving estimates of effective Q parameters. Similar to Figure 10, Figure 12 compares kriged grids the Lg Q_0 estimates. As noted, these grids are merely a convenient graphical representation of the spatial Q_0 variations for comparison. The grids have some very similar patterns, e.g., our results agree very well with those from Phillips for stations in Kazakhstan and Kyrgyzstan. The average of our Lg Q_0 estimates is 442 versus 478 from Phillips for the paths/stations shown. The largest differences are that our Q_0 values are 18% to 32% lower than those from Phillips for TLY, NIL, LZH, ULN, and WMQ. We plan to include more data to improve and validate our results. However, it is interesting that we obtain qualitatively similar results using only a single pair of events with well-constrained source terms.

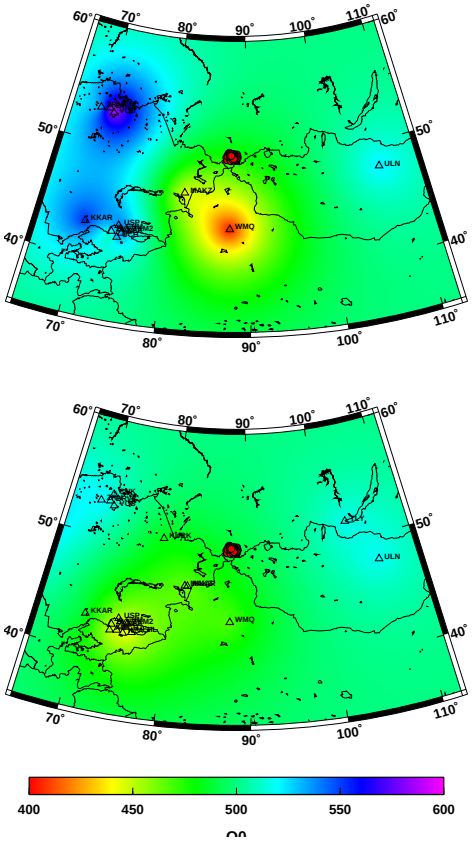

Figure 10. Interpolated grids of Lg Q_0 from our analysis (top) and from Xie (2008, pers. comm.) (bottom) for stations with recordings of the cluster shown in red. (These are not tomographic Q_0 maps. They represent the effective Q_0 along various paths.)

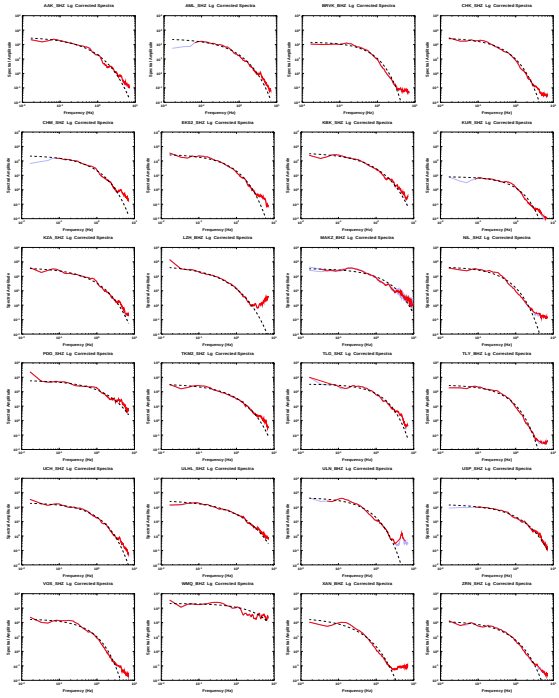

Figure 11. Source-corrected Lg spectra and Q model fits for LNTS earthquakes recorded by 24 stations.

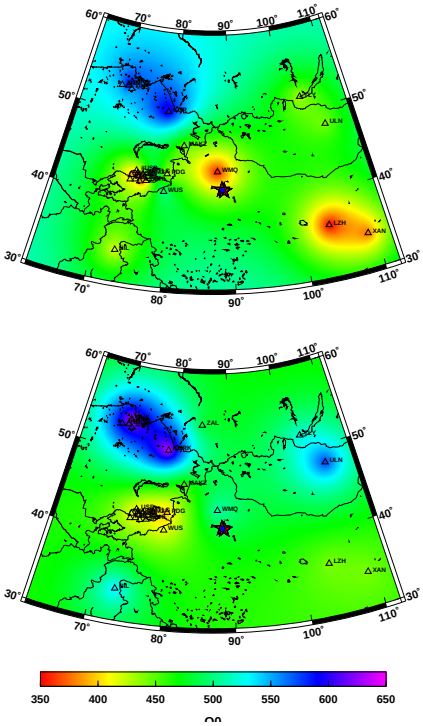

Figure 12. Interpolated grids of effective Lg Q_0 for paths from LNTS to regional stations from our analysis (top) and based on Q tomography (bottom).

New Work

The previous effort showed that, by first eliminating path and site effects, accurate source terms can be estimated and used to then reliably estimate combined distance and site dependence. This fully calibrates paths/stations with data. We are now extending the constrained approach to eliminate remaining trade-offs, to separate path and site effects. This will allow spatial interpolation and physical interpretation of estimated parameters, more meaningful comparisons to existing results, and to merge our results with existing models at LANL. Note, for example, that site corrections generally have frequency dependence, but the behavior varies by station and is not necessarily intuitive, as illustrated by different dependence for P and S waves for two stations (Figure 13). We need to assess whether this dependence real or due to a trade-off with Q. Inaccurate estimates of site effects will adversely impact Q estimates. As before, non-uniformity of the earth and the data complicate this matter. New work is planned to separately constrain site from distance terms.

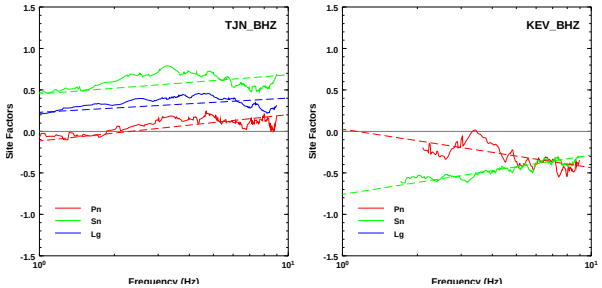

Figure 13. Site corrections for stations TJN in South Korea and KEV in Finland, computed as residuals of source- and distance-corrected spectra.

Figure 14 shows key processing steps of our approach, indicating several key aspects. First, for this project, we plan to greatly augment the dataset based on direct P and S phases from similar event pairs, by using Lg coda measurements. That is, in addition to the data depicted in Figure 6, we plan to use the coda measurements shown in Figure 15. Mayeda et al. (2007) have shown that coda measurements allow the criteria of similar events and locations to be relaxed, greatly increasing the number of observations. Phillips et al. (2008) used the Lg coda data of Figure 15 to invert for relative site and 2D path terms. We are using these complementary datasets, with coda providing greater density and direct phases providing information about P and S phases and allowing source term fits over broader frequencies, as shown above. We plan to (1) compare source terms estimated by different data and methods to validate them; (2) independently estimate site terms; and (3) to cross-validate and merge the final correction and uncertainty terms.

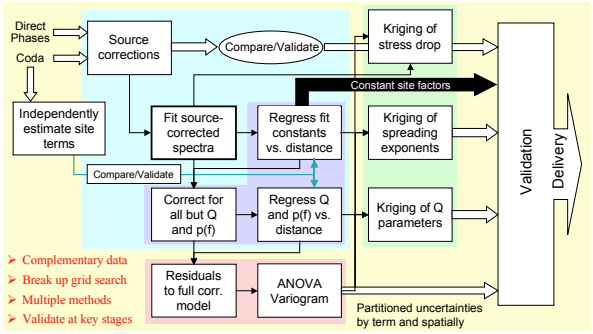

Figure 14. Schematic flow chart of planned analyses.

Second, we will further dissect the grid-search approach (represented by the large cyan box of Figure 15) into more manageable pieces. We have already accomplished part of the problem, giving source corrections for many events and fitting the source-corrected spectra. We will further break up the analysis of the three boxes (grouped in blue), as described further below. Third, we plan to use multiple methods within each of these boxes, to compare and validate the results at key stages. Other key aspects of the analyses are to partition the uncertainties, interpolate the physical parameters by kriging, and to merge our results with existing models.

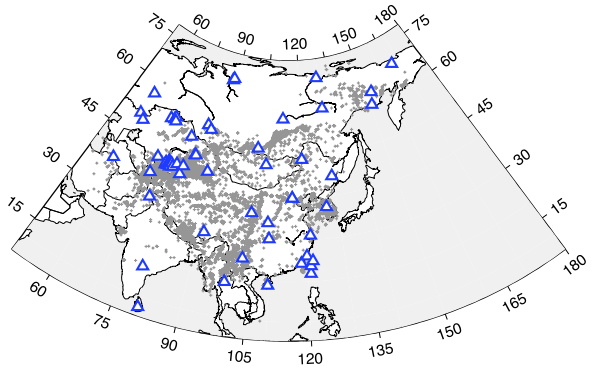

Figure 15. Stations (triangles) and events (crosses) used by LANL to calibrate Lg coda in east Asia.

To illustrate some details of the planned methods, note that the constant offsets of the model fits to the

source-corrected spectra (e.g., black dashed curves in Figures 9 and 11) depend on geometrical spreading and a constant site factor. Since the former depends on distance and the latter does not, we can regress the constants of the fits for all clusters/pairs of events recorded by a given station at different distances to separately constrain them. We plan to use larger datasets to perform this analysis.

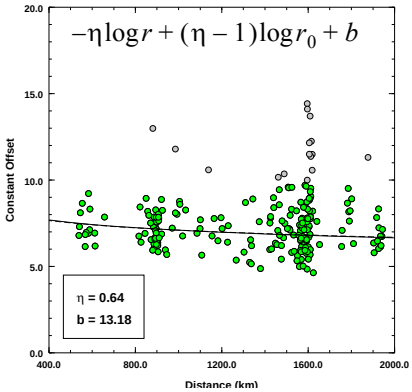

Figure 16. Constant terms of the model fits versus distance (circles) and regression versus log distance. Gray circles were excluded from the analysis. The legend lists the estimated values of the geometrical spreading exponent and the constant site factor.

Once we estimate these terms, the only parameters to be resolved are Q_0 , γ , and one that governs the frequency dependence of the site term. We have investigated various approaches for this final step. One is to insert the spectral amplitudes for all of the events in our datasets, now corrected for all but these terms, into a grid search for three parameters. This is a much smaller parameter space than the full space associated with Equation (1). As in separating the spreading and constant site terms, Q_0 and γ can be separated from the frequency-dependent site term by distance. A second approach, is to use constraints from coda measurements and methods to independently estimate (relative) site terms.

A third approach that imposes an additional constraint on these last three parameters, is to use relative spectra for clusters with similar paths, but at different distances from a station, to factor out the site term and obtain a robust estimate of Q for that path. This estimate of Q has no trade-off with source, site, or geometrical spreading effects. Figure 17 illustrates this approach. It shows the ratio of the median source-corrected spectra at MAKZ (Makanchi, Kazakhstan) for the two clusters along the path shown in Figure 6. This relative spectrum factors out the site term, and the spreading terms are different constants, i.e., independent of frequency. Assuming the effective Q is relatively constant over a path, the ratio of source-corrected median spectra for the two clusters is simply modeled by

$$\log(\tilde{A}_1 / \tilde{A}_2) = \frac{\pi f^{1-\gamma}}{Q_0 v} \Delta r \ , \qquad \text{(EQ 3)}$$

where Δr is the separation of the clusters. Fitting this expression to empirical spectral ratios (dashed curve in Figure 17) gives constrained estimates of Q_0 and γ (e.g., Lg $Q_0 = 546$ for the path depicted in Figure 6.

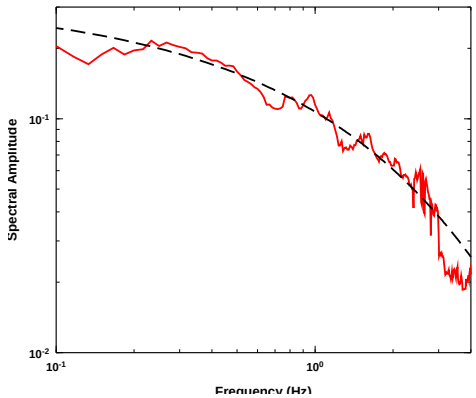

Figure 17. Ratio of source-corrected median spectra at MAKZ for two clusters along the great-circle path in Figure 6. The relative spectrum factors out the site term and allows a robust estimate of Q for this path.

Correcting the source-corrected spectra of these clusters now for Q, the remaining frequency dependence is due to site effects. Once this is done for at least one path, the frequency-dependent site term may be estimated and fixed, under the assumption of the standard model that $P(f)$ is independent of azimuth. We can then estimate Q for all paths with available data. The other assumption is that a suitable path exists for a given station along which Q is fairly constant. We need to investigate its validity for stations of interest, e.g., using existing tomographic maps as an *a priori* guideline. We refer to the overall approach as a stepwise, iterative procedure to constrain all of the parameters of the standard model, using our available datasets (Figures 6 and 15), source-corrected spectra, and model fits (e.g., Figure 9) as a starting point.

CONCLUSIONS AND RECOMMENDATIONS

This effort focuses on developing and testing methods to improve source, distance, and site correction parameters, and their uncertainties, for regional seismic phases. It has been well know for over a decade (e.g., Taylor and Hartse, 1998) that there are significant trade-offs among distance and source terms, using standard grid-search techniques to invert for all parameters simultaneously. We illustrated the problem for LNTS. Fisk and Taylor (2006) and Fisk et al. (2008) discuss additional cases by various researchers for which unconstrained inversion methods have led to large errors in both distance and source corrections. Such errors, and the potential impact on nuclear explosion monitoring using regional phases, motivated the development of our constrained approach to eliminate such trade-offs. Under a previous project, we developed and tested a method that first estimates source parameters using Brune model fits to relative spectra of regional phases for event pairs with similar mechanisms, but different moments. Using such relative spectra ensures that path and site effects cancel out, thereby allowing accurate estimation of the source terms. Once the spectra are corrected by reliable source terms, we can accurately estimate distance and site effects. We applied our constrained approach to two large datasets in Eurasia. We automated the various processing steps, including assessing event pairs from waveform cross-correlations, computing network-median of relative spectra (large over small events), and fitting the Brune model to estimate corner frequencies and stress drop. We used kriging to interpolate grids of stress drop for Eurasia. We compared these preliminary grids to existing ones at LANL. Further work is needed to interpret the stress-drop grids in terms of large-scale geophysical structure.

A key result of that research is that the relative spectra for a given earthquake pair are often quite similar for the various phases, although over different frequency ranges because of phase-dependent signal-to-noise limitations. Hence, the model fits and estimated corner frequencies for the various phases are very similar. This appears to be a fairly common and important phenomenon for the earthquakes analyzed. It allows a more robust approach of fitting Brune source parameters, using a broader range of frequencies, by combining relative spectra of regional P and S phases for earthquakes (e.g., the black dashed curve in Figure 3).

Correcting the spectra for the source terms, we then fit the combined distance and site effects for the various events and stations in our dataset, showing that good calibration of non-source-related physical effects (distance and site terms) may be obtained over a wide range of frequencies for paths with data. The estimates of the source terms from relative spectra and the fits to the median source-corrected spectra (viz. the black dashed curves in Figures 9 and 11) provide all information necessary to completely correct the spectra for all source, distance, and site effects. Thus, by first constraining the source terms, we are now able to fully calibrate paths/stations with suitable data. Of particular interest, we obtain very similar Lg Q_0 estimates for many paths from LNTS to regional stations, as well as some notable differences, using only a single pair of earthquakes with well-constrained source terms, as compared to estimates from a tomographic Q_0 map. Our results illustrate how even a small number of events with well constrained source terms provide comparable or improved estimates of Lg Q.

The focus of this new project, which has just started, is to extend the constrained inversion approach to eliminate remaining trade-offs among Q, geometrical spreading, and site terms that have different distance and frequency dependence. We refer to the approach as a stepwise, iterative procedure to constrain estimates of all of the correction parameters. Starting with our source-corrected spectra and the model fits, the procedure would separate the spreading and constant site factors, apply those corrections, and then resolve Q and frequency-dependent site terms. We illustrated some of the ideas for station MAKZ. This is expected to provide more accurate estimates of all of the physical parameters of Equation (1) than currently exist. We also plan to incorporate coda measurements and methods (1) to greatly augment the source terms estimated using spectra of direct phases, relaxing the restriction on event pairs with similar mechanisms; and (2) as a way to independently estimate site dependence. Other key aspects of this work are to quantify uncertainties, validate the results, merge our results with existing models, and deliver the results.

ACKNOWLEDGMENTS

We are grateful to Jiakang Xie for Lg Q_0 estimates and useful discussions. Seismic data from the IRIS DMC were used in this study.

REFERENCES

Brune, J. N. (1970). Tectonic stress and the spectra of seismic shear waves from earthquakes, *J. Geophys. Res.* 75: 4997–5009.

Fisk, M. D., G. D. McCartor, and S. R. Taylor (2008). Robust Magnitude, Distance, and Path-Specific Corrections for Regional Seismic Phases by Constrained Inversion and Enhanced Kriging Methods, ATK/NCR-0608-501, Final Technical Report.

Fisk, M. D. and S. R. Taylor (2006). Robust magnitude and path corrections for regional seismic phases in Eurasia by constrained inversion and enhanced kriging techniques, in *Proceedings of the 28th Seismic Research Review: Ground-Based Nuclear Explosion Monitoring Technologies,* LA-UR-06-5471, Vol. 1, pp. 15–24.

Mayeda, K. M., L. Malagnini, and W. R. Walter (2007). A new spectral ratio method using narrow band coda envelopes: evidence for non-self-similarity in the Hector Mine sequence, *Geophys. Res. Lett.* 34: L11303.

Phillips, W. S., R. J. Stead, G. E. Randall, H. E. Hartse, and K. Mayeda (2008). Source effects from broad area network calibration of regional distance coda waves, in Scattering of Short Period Waves in the Heterogeneous Earth, H. Sato and M.C. Fehler, Editors., D. P. and P. G. Richards (2004). Repeating seismic events in China, *Science* 303: 1176–1178.

Sereno T. J., S. R. Bratt, and T. C. Bache (1988). Simultaneous inversion of regional wave spectra for attenuation and seismic moment in Scandinavia, *J. Geophys. Res.* 93: 2019–2035.

Taylor, S. R., and H. E. Hartse (1998). A procedure for estimation of source and propagation amplitude corrections for regional seismic discriminants, *J. Geophys. Res.* 103: 2781–2789.

Taylor, S. R., A. A. Velasco, H. E. Hartse, W. S. Phillips, W. R. Walter, and A. J. Rodgers (2002). Amplitude corrections for regional seismic discriminants, *Pure and Appl. Geophys., Special Edition on Monitoring the Comprehensive Nuclear-Test-Ban Treaty: Seismic Event Discrimination and Identification*, 159: 623–650.

Walter, W. R. and S. R. Taylor (2002). A Revised Magnitude and Distance Amplitude Correction (MDAC2) Procedure for Regional Seismic Discriminants: Theory and Testing at NTS, *UCRL-ID-146882,* LA-UR-02-1008.

Xie, J., D. Schaff, and Y. Liu (2005). Tomographic mapping of Lg Q in eastern Asia, in *Proceedings of the 27th Seismic Research Review: Ground-Based Nuclear Explosion Monitoring Technologies,* LA-UR-05-6407, Vol. 1, pp. 242–248.

Xie, J., Z. Wu, R. Liu, D. Schaff, Y. Liu, and J. Liang (2006). Tomographic regionalization of crustal Lg Q in eastern Eurasia, *Geophys. Res. Lett.*, 33, L03315.